Materials Advances

ROYAL SOCIETY OF CHEMISTRY

COMMUNICATION

View Article Online
View Journal | View Issue

Check for updates

Cite this: *Mater. Adv.*, 2024, 5, 136

Received 7th September 2023,
Accepted 28th November 2023

DOI: 10.1039/d3ma00673e

rsc.li/materials-advances

Pore-interface engineering improves doxorubicin loading to triazine-based covalent organic framework†

Preeti Rathi,‡[a] Sumanta Chowdhury,‡*[b] Partha Pratim Das,[c] Anand Kumar Keshri,[a] Anubha Chaudhary[a] and Prem Felix Siril*[b]

High drug-loading capacity is the most advantageous property of porous nanocarriers for cancer therapy. Covalent organic frameworks (COFs) are a novel class of porous nanocarriers that have been explored for drug delivery because of their tuneable textural properties and pore-surface functionalization. The primary focus of this study is to determine the dominant factor influencing drug loading in COFs. These results highlight the importance of pore-wall functionalization over the surface area to achieve a high drug-loading capacity and better drug–COF interaction. *In vitro* biological studies confirmed the biocompatibility of bare COFs and the efficacy of doxorubicin-loaded COF in killing cancer cells. In essence, the findings of this study suggest focussing on drug–COF interactions rather than high crystallinity and surface area for enhanced drug loading.

The drug-loading capacity (DLC) is a crucial aspect of chemotherapeutic drug delivery. Porous anticancer drug nanocarriers[1] have been designed and used for this purpose.[2,3] In this regard, COFs are gaining attention owing to their organic backbones, excellent biocompatibility, and design flexibility.[4,5] COFs offer advantages[6,7] in terms of pore size, shape, volume, surface area, linkages,[8] and functionality, making them favourable for drug encapsulation and release.[9–11] Moreover, by controlling the size and morphology of COFs,[12] they can be made more suitable as drug carriers. While the influence of pore size[13] and topological design[14,15] on DLC is well-established in the literature, the role of surface area remains unclear. Some COFs with high surface areas demonstrated low DLC, while those with low surface areas exhibited impressive DLC. For instance, CF-25 COF, which possesses a BET surface area of 1791 $m^2 g^{-1}$, exhibited a low DLC of only 3 wt% for camptothecin.[16] Similarly, PCOF@PDA with a BET surface area of 520 $m^2 g^{-1}$ could load only 5.3 wt% of the Gamboic acid drug.[17] In contrast, Fe_3O_4@-COF[18] despite having a negligible BET surface area of ~52 $m^2 g^{-1}$, achieved remarkable DLC of 33.3 wt% for doxorubicin (DOX). This discrepancy calls for further investigation of other key factors influencing DLC in COFs, particularly pore-surface functionalization, and linkage design. Two major approaches for pore-wall modulation in COFs are considered: side-unit decoration[14,19] and heteroatomic doping.[20] The choice between maximizing the surface area or implementing pore surface functionalization is central to achieving a higher DLC in COFs. To address this issue, the present study aims to unravel the intertwined role of the surface area and pore functionality in COFs to optimize DLC.

Herein, two isoreticular COFs linked with β-ketoenamine[21,22] bonds were synthesized and named TzCOF (triazine-based COF) and NTzCOF (triazine-based COF doped with pyridyl heteroatoms). The synthesized COFs differ in terms of their backbone composition. NTzCOF exhibited slightly improved crystallinity, surface area and pore volume compared to TzCOF. These COFs were further loaded with the anticancer drug DOX to investigate the impact of pore-wall functionalization on DLC. Additionally, TzCOF was synthesized with enhanced crystallinity and surface area, named CTzCOF (triazine-based COF with high crystallinity), and loaded with DOX. The heteroatom-doped NTzCOF demonstrated a higher DLC than the TzCOF and CTzCOF. This study also addressed the often-overlooked issue of loaded drug-loss during the washing steps. This emphasized the actual strength of the interaction between the drug and nanocarrier. Furthermore, biocompatibility tests on non-cancerous human embryonic kidney cells (HEK 293T) were performed for bare nanocarriers. Cytotoxicity evaluation of human lung cancer cells (A549) was also performed for the DOX-loaded NTzCOF [DOX@NTzCOF]. A

[a] *School of Biosciences and Bioengineering and Bio-X Research Centre, Indian Institute of Technology Mandi, Mandi, 175005, Himachal Pradesh, India*
[b] *School of Chemical Sciences and Advanced Materials Research Centre, Indian Institute of Technology Mandi, Mandi, 175005, Himachal Pradesh, India. E-mail: chowdhuryraj.92@gmail.com, prem@iitmandi.ac.in*
[c] *Department of Chemistry, Manipal Institute of Technology, Manipal Academy of Higher Education, Manipal, 576104, Karnataka, India*

† Electronic supplementary information (ESI) available. See DOI: https://doi.org/10.1039/d3ma00673e

‡ S. C. and P. R. have equally contributed to this work.

time-dependent increase in cellular uptake of the nanocarrier by A549 cells was observed.

Tritopic aldehyde and amine were first synthesized in the laboratory following reported procedures (ESI,† S2.1 and S2.2). Subsequently, β-ketoenamine linked organic polymers, TzCOF,[23] and NTzCOF,[24] were synthesized *via* a Schiff-base condensation reaction using a solvothermal synthetic procedure with slight modifications (ESI,† S2.3). The isoreticular COFs differed only in terms of the heteroatomic pyridyl nitrogen doping (Scheme 1). The characteristic peaks for C=O, C=C, and C–N stretching in the FTIR spectra confirmed the successful synthesis of organic polymers (Fig. S3a, 3b and 3c, ESI†). In addition, disappearance of the characteristic peaks of –N–H and –CHO confirmed the absence of any residual monomers or oligomers.

Materials Studio software was used to simulate the crystal structures of the COFs by optimizing the lattice parameters in *P*1(1) space groups with AA and AB stacking. The simulated X-ray diffraction (XRD) patterns of the slipped AA stacking model (Fig. 1a–c) closely matched the experimental XRD patterns, indicating a strong resemblance between the two. Intense peaks at 2θ = ~5.65–5.7° and a minor peak at 9.75–9.95° can be attributed to the presence of (100) and (110) reflection planes, respectively (Fig. 1b).[25] The broad peak at 2θ = ~26.5–27.1° corresponds to the (001) reflection plane (Fig. 1b). As shown in Fig. 1a–c, CTzCOF had the highest crystallinity among the polymers (Fig. 1b). Further, the crystallinity of NTzCOF (Fig. 1c) was better than that of TzCOF (Fig. 1a). Additionally, the experimental PXRD patterns were successfully refined using Rietveld analysis, showing excellent agreement with theoretically simulated models of slipped AA stacking. The corresponding datasets are listed in Table S1 (ESI†).

Both the TzCOF-based nanocarriers showed Type-I isotherms while the NTzCOF showed a Type-IV isotherm due to the presence of mesoporous defects in the structure[26,27] (Fig. 1c). CTzCOF exhibited the highest BET surface area of 1205 $m^2\ g^{-1}$ whereas NTzCOF and TzCOF exhibited surface areas of 768 and 644 $m^2\ g^{-1}$, respectively (Fig. 1d). The microporous nature of the isoreticular COFs with a pore size of ~1.4 nm was evident from their QSDFT pore size distribution (Fig. 1e). The micropore volumes of TzCOF, CTzCOF and NTzCOF were 0.14, 0.37 and 0.18 cc/g respectively (Table S2, ESI†).

Furthermore, the particle size of a nanocarrier is an important factor that affects its biodistribution and uptake by the cells.[28] Transmission electron microscopy (TEM) images revealed that TzCOF and NTzCOF exhibit a nanofibrous structure (depicted in Fig. 1f), displaying average particle diameters of 16 ± 4.2 nm and 50 ± 7.2 nm, and lengths of 110 ± 19 nm

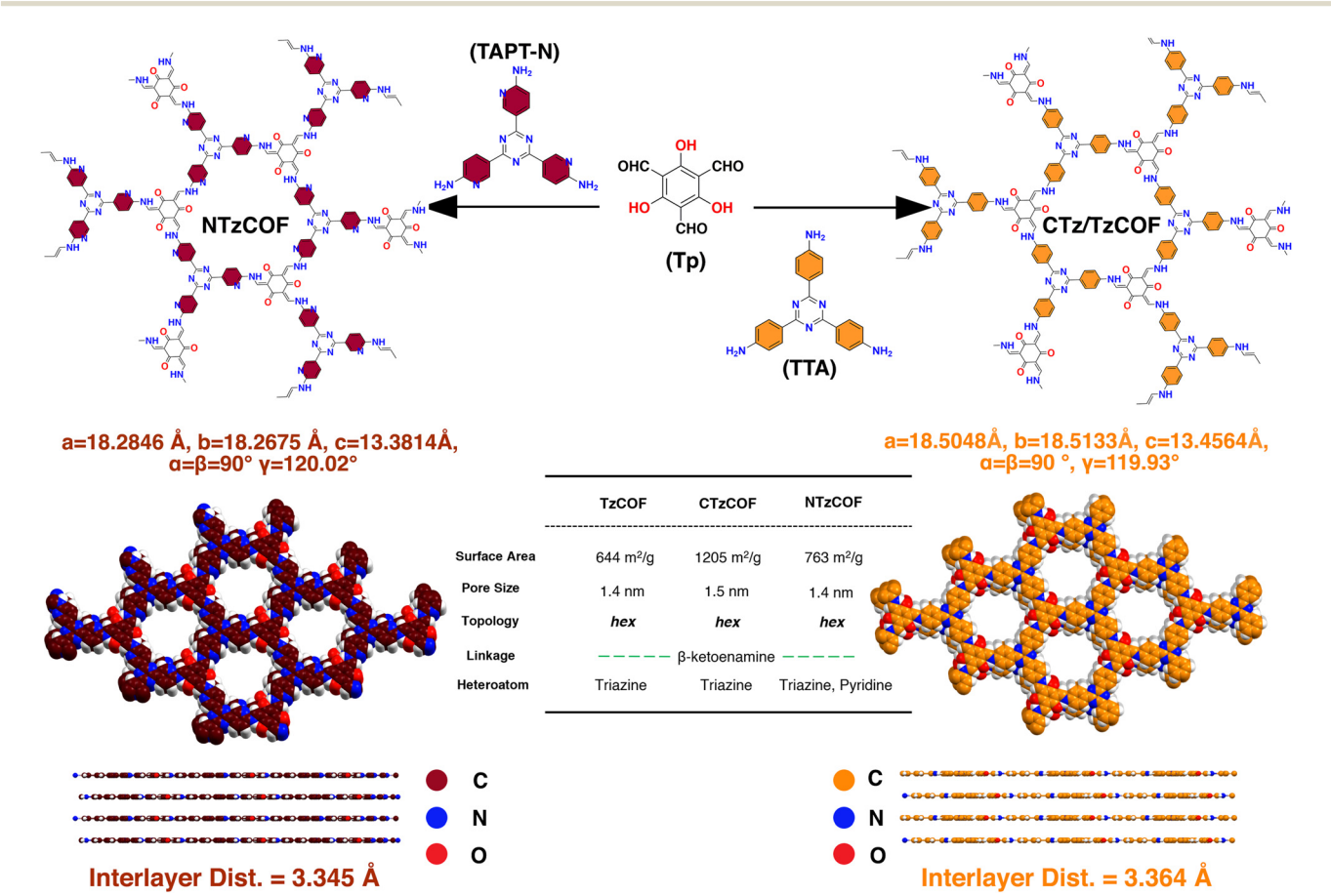

Scheme 1 Schematic representation of isoreticular COFs with different backbone compositions.

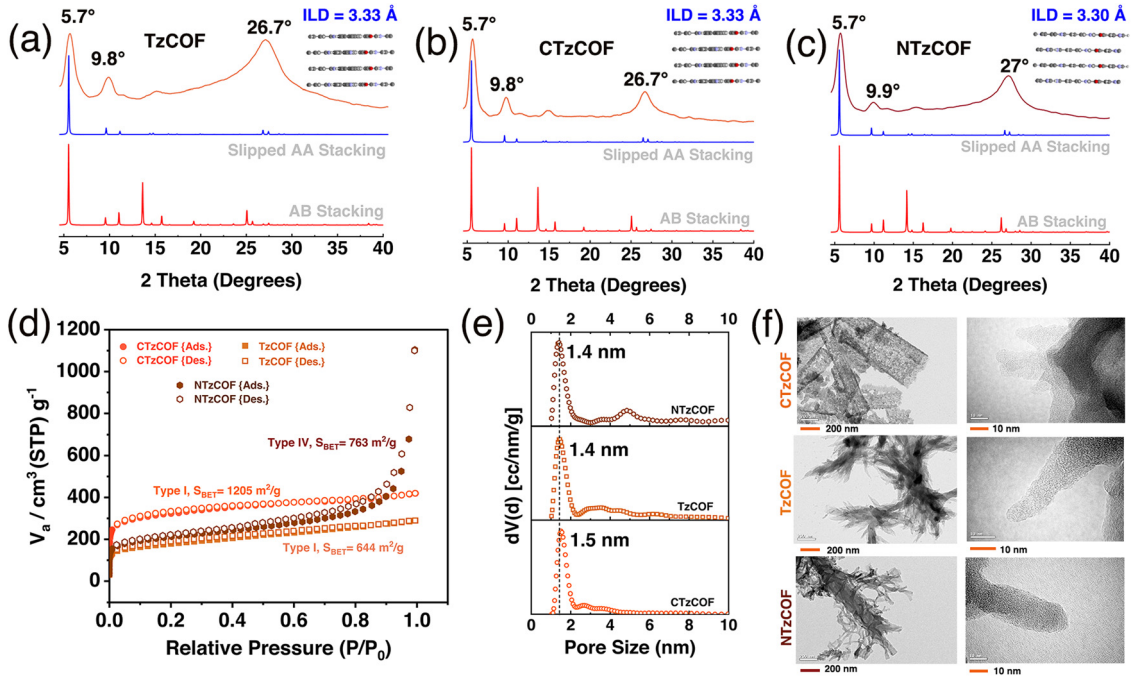

Fig. 1 XRD patterns of (a) TzCOF, (b) CTzCOF, and (c) NTzCOF along with their simulated slipped AA stacking patterns. (d) N_2 adsorption isotherms of COFs along with their (e) statistical pore-size distribution (QSDFT method, cylindrical pore, and N_2 on carbon at 77 K). (f) TEM images.

and 81 ± 15 nm, respectively (Fig. S6, ESI†). However, CTzCOF possessed sheet-like morphology with larger particle sizes as shown in Fig. 1f. Hence, the nanofibrous TzCOF and NTzCOF are in a suitable size range for enhanced permeable retention (EPR) effect.[29] Surface charge also plays a significant role in the biodistribution and cellular uptake of drug-delivery systems.[30] ZP measurements of the bare and drug-loaded nanocarriers were performed in water (25 °C), PBS (25 °C), and Dulbecco's

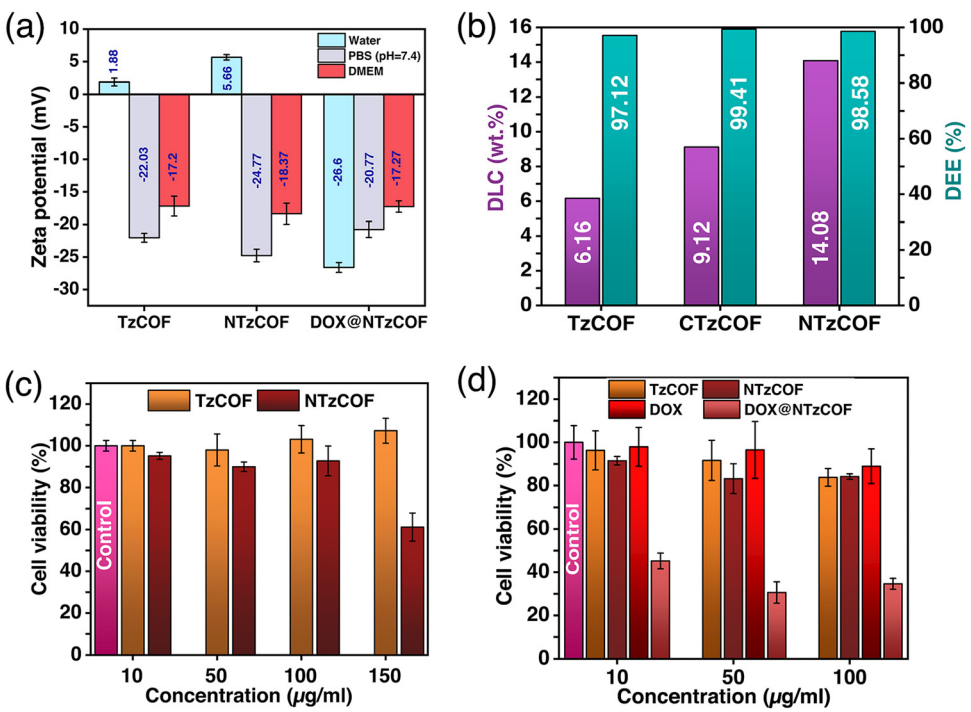

Fig. 2 Bar graphs showing (a) ZP of bare and drug-loaded COFs, (b) DLC and DEE comparison of three nanocarriers, (c) biocompatibility of bare nanocarriers for HEK 293T cells and (d) comparative cytotoxicity of bare nanocarriers, only DOX (1.4, 7 and 14 μg mL^{-1} as per the DLC of NTzCOF) and DOX@NTzCOF for A549 cells.

modified Eagle's medium (DMEM) (37 °C).[31] The mean ZP values of TzCOF, NTzCOF and DOX@NTzCOF in DMEM (37 °C) were −17.2, −18.37 and −17.27 mV, respectively (Fig. 2a), indicating the stability of nanocarrier dispersion for *in vitro* cell culture experiments. The π-conjugation in the COF structure provides a fluorescence nature to COFs.[32] Both the nanocarriers showed fluorescence emission in water at excitation wavelengths of 472 nm for NTzCOF and 425 nm for TzCOF (Fig. S7, ESI†).

DOX was loaded into the nanocarriers using a post-synthetic drug-loading strategy (ESI,† S3).[33,34] The drug-loaded nanocarriers were then collected by centrifugation followed by several washings, and DLC was quantified by UV-Vis spectroscopy (ESI,† Scheme S3). The UV-visible absorbance spectra of DOX before and after loading are shown in Fig. S8a–c (ESI†). The DLC was calculated to be 13.04, 17.19 and 21.99 wt% for TzCOF, CTzCOF and NTzCOF, respectively. However, the DLC decreased to 6.16, 9.12 and 14.08 wt% for TzCOF, CTzCOF and NTzCOF, respectively after three subsequent washings with distilled water. Fig. S9 (ESI†) shows the change in the DLC of the three COFs with the subsequent washings. A comparison of the DLC and drug encapsulation efficiency (DEE) of the three COFs with other materials for DOX delivery is given in Table S3 (ESI†).

Overall, NTzCOF showed better DOX-loading capacity than the other two COFs (Fig. 2b). Thus, the pyridyl heteroatoms seem to be the dominant factor determining DLC in the COFs rather than crystallinity, surface area and pore volume. The molecular dimension of DOX is 1.46 × 1.0 × 0.69 nm.[35] Therefore, it is possible for the drug molecules to enter the pores of COFs (∼1.5 nm) through the smallest dimension and get absorbed on the internal surface of COFs. FTIR (Fig. S10, ESI†) and XPS (Fig. S11 and S12, ESI†) were also performed to confirm DOX-loading. The emergence of FTIR peaks at 1414 and 987 cm^{-1} in the DOX-loaded NTzCOF confirms the presence of the drug molecule inside the pores.[36] XPS spectra showed signals associated with the C–O and C–NH_3^+ functionalities of DOX. These signals appeared at binding energies of ∼531 (Fig. S11, ESI†) and ∼401 eV (Fig. S12, ESI†), respectively, which were absent in the case of pristine COFs.[37] Moreover, the change in the surface charge of NTzCOF from +5.66 to −26.6 mV for DOX@NTzCOF (Fig. 2a) also supports successful drug-loading.[38,39] The change in the surface charge of the COFs after drug loading could be attributed to the interaction between the cationic DOX and the Lewis basic pyridinic nitrogen present in NTzCOF.[40,41] FTIR, XPS and ZP also provide insight into the dominance of pyridyl heteroatoms for high DLC (Fig. S10–S12 (ESI†) and Fig. 2a).

After completing the assessment of DLC and the necessary characterization, TzCOF and NTzCOF were employed for *in vitro* biological studies. The 3-(4,5-dimethylthiazol-2-yl)-2,5-diphenyl tetrazolium bromide (MTT) assay was performed to evaluate the biocompatibility of bare nanocarriers and the cytotoxicity of DOX@NTzCOF (ESI,† S4.1–S4.3).[42] CTzCOF was not used for biological studies as it is similar to TzCOF, except for crystallinity, surface area and pore volume. Moreover, it had a completely different morphology and a larger particle size. The biocompatibilities of bare TzCOF and NTzCOF were studied in HEK 293 cells. Both nanocarriers showed non-significant cell death at concentrations up to 100 μg mL^{-1}. However, NTzCOF exhibited considerable cytotoxicity at 150 μg mL^{-1} (Fig. 2c). Further, the cytotoxicity of TzCOF,

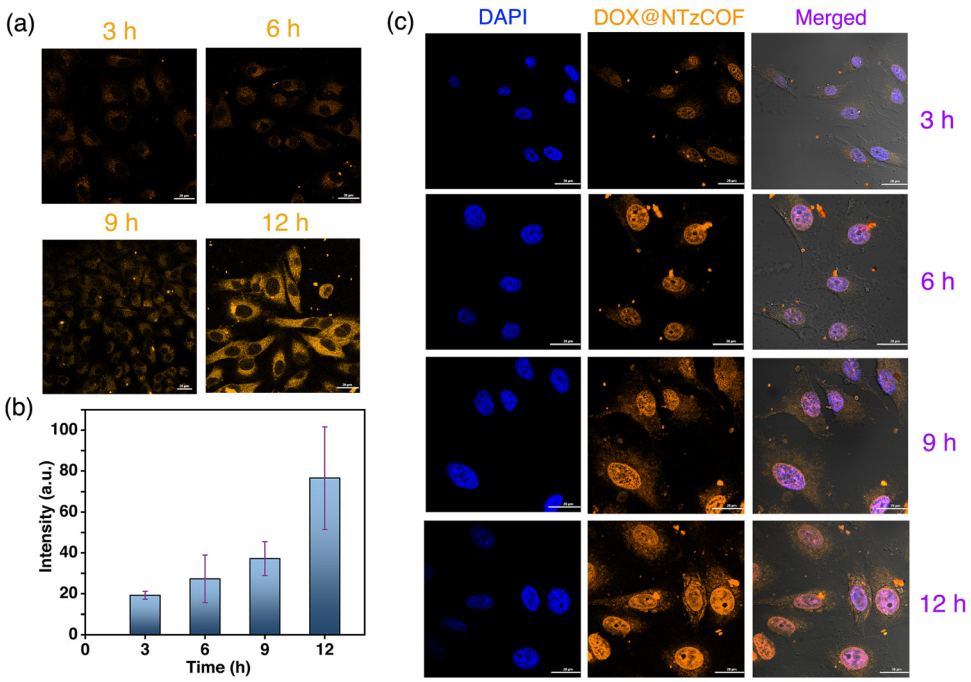

Fig. 3 (a) Confocal images showing the uptake of bare NTzCOF by A549 cells. (b) Bar graph showing time-dependent fluorescence intensity of NTzCOF in A549 cells. (c) Confocal images of A549 cells treated with DOX@NTzCOF.

NTzCOF, DOX@NTzCOF and DOX was analysed in A549 cells (Fig. 2d). Similar to the results in HEK 293 cells, the bare COFs did not show any significant cytotoxicity against A549 at concentrations ranging from 10 to 100 μg mL^{-1}. However, DOX@NTzCOF reduced the cell viability up to 46% even at its lowest concentration of 10 μg mL^{-1}. Further, the cytotoxicity of DOX@NTzCOF was compared with that of DOX as a control. Dosage amount of DOX were chosen according to the DLC of the NTzCOF. The cell-killing ability of DOX@NTzCOF was much higher than that of DOX at equivalent concentrations confirming the efficient drug delivery into the cells. Furthermore, confocal laser scanning microscopy (CLSM) was performed to determine the relevance of the MTT assay results to the cellular uptake of DOX@NTzCOF.

A549 cells were treated with the pristine fluorescent NTzCOF nanocarrier, and CLSM images were captured at different time points (Fig. 3a). Details of the treatments and sample preparation for imaging are provided in the ESI† (Section S4.4). Additionally, quantitative fluorescence intensity measurements were conducted, and the results indicated the increasing uptake of NTzCOF nanocarriers with time (Fig. 3b).

Images were captured at different *z*-heights to confirm the cellular uptake of the nanocarriers (Fig. S13, ESI†). After confirming the uptake of NTzCOF, the drug-delivery efficacy of the nanocarrier was visualized using CLSM. Confocal images of A549 cells treated with DOX@NTzCOF were obtained at different time intervals (Fig. 3c). The results were further compared with those of DOX-treated A549 cells (Fig. S14, ESI†). It was observed that the NTzCOF nanocarrier efficiently delivered the drug into the cells within 3 h. This was evident from the fluorescence intensity of DOX inside the cell nucleus, which was observed using the TRITC emission filter.[32,43] The fluorescence intensity of DOX inside the nucleus increased with time. This can be related to the continuous delivery of DOX by DOX@NTzCOF as their uptake by the cells increased with time.

In conclusion, this study sheds light on the significance of pore-interface tuning in COFs, which is more significant than their surface area and crystallinity for achieving enhanced drug-loading capacity. The present study also underscores the crucial role of the interactions between drugs and nanocarriers in preventing drug loss from the loaded system. Moreover, the synthesized COF-nanocarriers exhibited promising efficacy in anticancer drug delivery, as corroborated by *in vitro* biological studies. In short, these results highlight the potential advantages of using purposefully modified amorphous covalent organic polymers over traditional COFs. The results of the *in vitro* biological studies of NTzCOF indicate the possibility of assessing its potential for *in vivo* studies. However, it is essential to precisely control the particle size, morphology, and linkage design, and, most significantly, ensure superior dispersibility.

Author contributions

P. R.: reproduction of nanocarrier synthesis, drug loading and release studies, *in vitro* biological studies, fluorescence imaging and analysis, data curation, manuscript writing. S. C.: ideation, experimental design, synthesis of monomers and COF nanocarriers, characterization, electron microscopy, data curation, manuscript editing. P. P. D.: Rietveld refinement of the experimental COF crystal structures. A. K. K.: biological experiments. A. C.: biological experiments. P. F. S. has acquired funding, supervised the presented study, reviewed and finalised the manuscript.

Conflicts of interest

The authors declare no conflict of interest.

Acknowledgements

The authors acknowledge the AMRC and Bio-X Research Centre for providing research facilities. PR acknowledges the Department of Science and Technology (DST-INSPIRE) India, for funding. Dr. Amit Prasad (Associate Professor, School of Biosciences and Bioengineering, IIT Mandi, India) is sincerely acknowledged for funding and guidance in biological studies. Dr. Abhishek Sharma (School of Physics and CRANN Institute, Trinity College Dublin, Dublin 2, Ireland) is sincerely acknowledged for simulating the Covalent Organic Framework structures used in this study.

References

1 S. Chowdhury, P. Sharma, K. Kundu, P. P. Das, P. Rathi and P. F. Siril, Systematic Thiol Decoration in a Redox-Active UiO-66-$(SH)_2$ Metal–Organic Framework: A Case Study under Oxidative and Reductive Conditions, *Inorg. Chem.*, 2023, **62**, 3875–3885.
2 M. Gong, J. Yang, Y. Li and J. Gu, Glutathione-responsive nanoscale MOFs for effective intracellular delivery of the anticancer drug 6-mercaptopurine, *Chem. Commun.*, 2020, **56**, 6448–6451.
3 M. C. Scicluna and L. Vella-Zarb, Evolution of nanocarrier drug-delivery systems and recent advancements in covalent organic framework–drug systems, *ACS Appl. Nano Mater.*, 2020, **3**, 3097–3115.
4 L. Huang, J. Yang, Y. Asakura, Q. Shuai and Y. Yamauchi, Nanoarchitectonics of Hollow Covalent Organic Frameworks: Synthesis and Applications, *ACS Nano*, 2023, **17**, 8918–8934.
5 J. Yang, L. Huang, J. You and Y. Yamauchi, Magnetic Covalent Organic Framework Composites for Wastewater Remediation, *Small*, 2023, **19**, 2301044.
6 A. Kumar Mahato, S. Pal, K. Dey, A. Reja, S. Paul, A. Shelke, T. G. Ajithkumar, D. Das and R. Banerjee, Covalent Organic Framework Cladding on Peptide-Amphiphile-Based Biomimetic Catalysts, *J. Am. Chem. Soc.*, 2023, **145**, 12793–12801.
7 S. Paul, M. Gupta, K. Dey, A. K. Mahato, S. Bag, A. Torris, E. B. Gowd, H. Sajid, M. A. Addicoat, S. Datta and R. Banerjee, Hierarchical covalent organic framework-foam

for multi-enzyme tandem catalysis, *Chem. Sci.*, 2023, **14**, 6643–6653.
8 S. Liu, J. Yang, R. Guo, L. Deng, A. Dong and J. Zhang, Facile fabrication of redox-responsive covalent organic framework nanocarriers for efficiently loading and delivering doxorubicin, *Macromol. Rapid Commun.*, 2020, **41**, 1900570.
9 S. Bhunia, K. A. Deo and A. K. Gaharwar, 2D Covalent Organic Frameworks for Biomedical Applications, *Adv. Funct. Mater.*, 2020, **30**, 2002046.
10 C. Liao and S. Liu, Tuning the physicochemical properties of reticular covalent organic frameworks (COFs) for biomedical applications, *J. Mater. Chem. B*, 2021, **9**, 6116–6128.
11 C. Valenzuela, C. Chen, M. Sun, Z. Ye and J. Zhang, Strategies and applications of covalent organic frameworks as promising nanoplatforms in cancer therapy, *J. Mater. Chem. B*, 2021, **9**, 3450–3483.
12 H. S. Sasmal, A. Kumar Mahato, P. Majumder and R. Banerjee, Landscaping Covalent Organic Framework Nanomorphologies, *J. Am. Chem. Soc.*, 2022, **144**, 11482–11498.
13 L. Li, Q. Yun, C. Zhu, G. Sheng, J. Guo, B. Chen, M. Zhao, Z. Zhang, Z. Lai, X. Zhang, Y. Peng, Y. Zhu and H. Zhang, Isoreticular Series of Two-Dimensional Covalent Organic Frameworks with the kgd Topology and Controllable Micropores, *J. Am. Chem. Soc.*, 2022, **144**, 6475–6482.
14 W. Zhao, C. Yu, J. Zhao, F. Chen, X. Guan, H. Li, B. Tang, G. Yu, V. Valtchev, Y. Yan, S. Qiu and Q. Fang, 3D Hydrazone-Functionalized Covalent Organic Frameworks as pH-Triggered Rotary Switches, *Small*, 2021, **17**, 2102630.
15 S. Karak, S. Kumar, P. Pachfule and R. Banerjee, Porosity Prediction through Hydrogen Bonding in Covalent Organic Frameworks, *J. Am. Chem. Soc.*, 2018, **140**, 5138–5145.
16 A. D. S. Oliveira, E. M. Rivero-Buceta, C. Vidaurre-Agut, A. Misturini, V. Moreno, J. L. Jordá, G. Sastre, S. B. C. Pergher and P. Botella, Sequential pore wall functionalization in covalent organic frameworks and application to stable camptothecin delivery systems, *Mater. Sci. Eng., C*, 2020, **117**, 111263.
17 J. Feng, W.-X. Ren, F. Kong, C. Zhang and Y.-B. Dong, Nanoscale covalent organic framework for the low-temperature treatment of tumor growth and lung metastasis, *Sci. China Mater.*, 2022, **65**, 1122–1133.
18 K. Zhao, P. Gong, J. Huang, Y. Huang, D. Wang, J. Peng, D. Shen, X. Zheng, J. You and Z. Liu, Fluorescence turn-off magnetic COF composite as a novel nanocarrier for drug loading and targeted delivery, *Microporous Mesoporous Mater.*, 2021, **311**, 110713.
19 R. Liu, L. Huang, H. Tao, X. Lei and Q. Shuai, Microenvironment engineering of covalent organic frameworks for the efficient removal of sulfamerazine from aqueous solution, *J. Environ. Chem. Eng.*, 2022, **10**, 107300.
20 A. Putta Rangappa, D. Praveen Kumar, K. H. Do, J. Wang, Y. Zhang and T. K. Kim, Synthesis of Pore-Wall-Modified Stable COF/TiO_2 Heterostructures via Site-Specific Nucleation for an Enhanced Photoreduction of Carbon Dioxide, *Adv. Sci.*, 2023, **10**, 2300073.
21 S. Kandambeth, A. Mallick, B. Lukose, M. V. Mane, T. Heine and R. Banerjee, Construction of Crystalline 2D Covalent Organic Frameworks with Remarkable Chemical (Acid/Base) Stability via a Combined Reversible and Irreversible Route, *J. Am. Chem. Soc.*, 2012, **134**, 19524–19527.
22 S. Mitra, H. S. Sasmal, T. Kundu, S. Kandambeth, K. Illath, D. Diaz Diaz and R. Banerjee, Targeted drug delivery in covalent organic nanosheets (CONs) via sequential postsynthetic modification, *J. Am. Chem. Soc.*, 2017, **139**, 4513–4520.
23 W. Li, C.-X. Yang and X.-P. Yan, A versatile covalent organic framework-based platform for sensing biomolecules, *Chem. Commun.*, 2017, **53**, 11469–11471.
24 S. Haldar, R. Kushwaha, R. Maity and R. Vaidhyanathan, Pyridine-Rich Covalent Organic Frameworks as High-Performance Solid-State Supercapacitors, *ACS Mater. Lett.*, 2019, **1**, 490–497.
25 R. Gomes and A. Bhaumik, A new triazine functionalized luminescent covalent organic framework for nitroaromatic sensing and CO_2 storage, *RSC Adv.*, 2016, **6**, 28047–28054.
26 J. Andersson, J. Rosenholm, S. Areva and M. Lindén, Influences of Material Characteristics on Ibuprofen Drug Loading and Release Profiles from Ordered Micro- and Mesoporous Silica Matrices, *Chem. Mater.*, 2004, **16**, 4160–4167.
27 C. G. Bavnhøj, M. M. Knopp, C. M. Madsen and K. Löbmann, The role interplay between mesoporous silica pore volume and surface area and their effect on drug loading capacity, *Int. J. Pharm. X*, 2019, **1**, 100008.
28 X. Duan and Y. Li, Physicochemical Characteristics of Nanoparticles Affect Circulation, Biodistribution, Cellular Internalization, and Trafficking, *Small*, 2013, **9**, 1521–1532.
29 R. Zein, W. Sharrouf and K. Selting, Physical Properties of Nanoparticles That Result in Improved Cancer Targeting, *J. Oncol.*, 2020, **2020**, DOI: **10.1155/2020/5194780**.
30 S. Honary and F. Zahir, Effect of Zeta Potential on the Properties of Nano-Drug Delivery Systems-A Review (Part 1), *Trop. J. Pharm. Res.*, 2013, **12**(2), 265–273.
31 I. Kaur, L.-J. Ellis, I. Romer, R. Tantra, M. Carriere, S. Allard, M. Mayne-L'Hermite, C. Minelli, W. Unger, A. Potthoff, S. Rades and E. Valsami-Jones, Dispersion of Nanomaterials in Aqueous Media: Towards Protocol Optimization, *JoVE*, 2017, e56074.
32 B. Wang, X. Liu, P. Gong, X. Ge, Z. Liu and J. You, Fluorescent COFs with a highly conjugated structure for visual drug loading and responsive release, *Chem. Commun.*, 2020, **56**, 519–522.
33 Y. Liu, G. Yang, S. Jin, L. Xu and C.-X. Zhao, Development of High-Drug-Loading Nanoparticles, *ChemPlusChem*, 2020, **85**, 2143–2157.
34 P. Gao, X. Shen, X. Liu, Y. Chen, W. Pan, N. Li and B. Tang, Nucleic Acid-Gated Covalent Organic Frameworks for Cancer-Specific Imaging and Drug Release, *Anal. Chem.*, 2021, **93**, 11751–11757.
35 I. B. Vasconcelos, T. G. da Silva, G. C. G. Militão, T. A. Soares, N. M. Rodrigues, M. O. Rodrigues, N. B. da Costa, R. O. Freire and S. A. Junior, Cytotoxicity and slow

release of the anti-cancer drug doxorubicin from ZIF-8, *RSC Adv.*, 2012, **2**, 9437–9442.

36 R. Bansal, R. Singh and K. Kaur, Quantitative analysis of doxorubicin hydrochloride and arterolane maleate by mid IR spectroscopy using transmission and reflectance modes, *BMC Chem.*, 2021, **15**, 27.

37 D. Y. Osadchii, A. I. Olivos-Suarez, A. V. Bavykina and J. Gascon, Revisiting Nitrogen Species in Covalent Triazine Frameworks, *Langmuir*, 2017, **33**, 14278–14285.

38 Y. Zhao, W. Xue, Z. Jiang, D. Liu, C. Hu and H. Huang, Construction of a Cationic Pyridinium-Based Covalent Triazine Framework for Ultra-fast and Efficient Iodine Adsorption, *ACS Sustainable Chem. Eng.*, 2023, **11**, 6741–6751.

39 M. Wang, P. Zhang, X. Liang, J. Zhao, Y. Liu, Y. Cao, H. Wang, Y. Chen, Z. Zhang, F. Pan, Z. Zhang and Z. Jiang, Ultrafast seawater desalination with covalent organic framework membranes, *Nat. Sustainable*, 2022, **5**, 518–526.

40 J. Yu, X. Jia, Y. Yang, C. Zhang, Y. Liu, D. Gao, Y. Fan and W. Li, Molecular dynamics study of a covalent organic framework as highly-efficient and biocompatible carriers for doxorubicin delivery: the role of nanopores, *J. Phys. D: Appl. Phys.*, 2021, **55**, 105402.

41 S. Fajal, D. Majumder, W. Mandal, S. Let, G. K. Dam, M. M. Shirolkar and S. K. Ghosh, Unraveling mechanistic insights into covalent organic frameworks for highly efficient sequestration of organic iodides from simulated nuclear waste, *J. Mater. Chem. A*, 2023, DOI: **10.1039/D3TA04995G**.

42 M. A. M. Shafiee, M. A. M. Asri and S. S. S. Alwi, Review on the In Vitro Cytotoxicity Assessment in Accordance to the International Organization for Standardization (ISO), *Malaysian J. Med. Heal. Sci.*, 2021, **17**(2), 261–269.

43 R. Liu, Supramolecular nanoparticles generated by the self-assembly of polyrotaxanes for antitumor drug delivery, *Int. J. Nanomed.*, 2012, **7**, 5249–5258.